CHAPTER – 5

Size dependent Melting temperature, Catalytic activation energy and Glass transition temperature of free and embedded soft matter

5.1 Introduction

The minuscule living organisms viruses and bacteria occur with different shapes and sizes in nature. Nonetheless, most of the viruses tend to be in spherical shapes with diameter ranging amidst 20–100 nm. All viruses are infinitesimal pockets of protein coat (capsid) which encloses nucleic acid core composed of either DNA or RNA. These tiny viruses have found promising applications in several fields of rapidly growing nanotechnologies[1]. In past years, the application of biological objects including viruses and bacteria as nanotemplates in nanofabrication was acquired[2,3,4,5,6]. For instance, tobacco mosaic virus (TMV) and M13 bacteriophage were successfully used in the synthesis of metallic and semiconductor nanowires[6]. For nanomaterial's self-assembly, inherently mutated TMV and M13 were well used[3]. Furthermore, the physical properties of TMV make it an attractive molecule for engineering hybrid materials[2]. Metal-coated TMVs have been used as a structural component in nickel-zinc and lithium ion batteries while TMV coated with fine platinum is a promising anode material for direct methanol fuel cells[4]. The utilization of viruses commonly occurs in two categories (i) major fabrication for bulk devices such as energy generation/storage, or ferrofluids; (ii) manufacturing of fine layers or wires for biosensors in the form of small quantity[2]. The researchers have successfully used genetically engineered viruses in contrast to the usual high-tech materials or microchips to harvest solar energy[5]. In addition, the common viruses have been found useful in producing materials that resemble skin and bone[7]. The evaluation of physical and chemical properties of viruses has been extensively explored[8,9] and topic of interest due to their budding use in nanotechnology and therapeutics. An insight in their mechanism is gaining many attentions in order to utilize

them in nanotechnology[10,11,12]. Our study will help in making predictions about biological phenomena and determining their properties relevant to nanotechnology design efforts and new therapeutic targets. Through low-frequency vibration analysis one can find its application in diagnosis/treatment of various viral diseases. The concept of killing and destroying viruses can be supported by the Rife therapy performed by a Rife frequency instrument, which destroys the microbe when there is a resonance between the mechanical oscillation frequency. The existence of well-defined resonance has also been emphasized by Ford[13] for which the knowledge of damping and width of the resonance is important and could be valuable for science and medicine. Another analogy to this is An Opera Singers voice which can break a thin crystal glass if the signal can match the glass natural frequency. Production and functioning of viruses can be better when the physical properties such as melting temperature, glass transition temperature and catalytic activation energy are well known both in free and embedded conditions. The study of glass transition temperature (T_g) for nanomaterials has been a subject of extensive attraction from last few years due to their significantly important applications. The particular interest however developed when a depression was first observed for small molecule glass formers confined in nanoporous glasses[14]. Nevertheless, there exists reports which claim enhancement in T_g for confined glass formers[15]. Glass transition temperature (T_g) of a material is not only important for its mechanical properties but also for many applications including to know the maximum usable temperature of the material. Furthermore, this is especially important for nanotechnologies that use polymeric thin films, using advanced integrated circuits[16].

It has been found that the finite size of a material affects its glass transition state and solubility[17]. Recently, the denatured hen egg white lysozyme, a highly basic protein has been found an effective tool for the solubilization of fullerene[18]. The melting temperature behavior of nanoparticles has attracted notable attentions and has been broadly studied[19,20,21]. In several areas, viruses are made to be active and inactive according to their need based applications. In this context, information about the thermodynamical parameter, melting temperature of the virus is important to be known before its application. Recently, Ku et al[22] predicted the melting temperature directly from protein sequencing. It

is observed that the proteins can be inactivated by high temperature. Hence, an accurate determination of the onset temperature at which proteins are irreversibly inactivated is of great importance to both protein science and the pharmaceutical industries[23]. The protein melting (T_m) is defined as the temperature at which the protein denaturation occurs. The protein denaturation very much depends on its size modification. Protein denaturation comprises an alteration in the protein structure (ordinarily an unfolding) with the loss of activity[24]. The area of nanocatalysis has been an active area of research from past many years[25]. The enzyme molecule lowers the activation energy of the reaction and increases its rate[26]. Furthermore, the lysozyme functionalized bioactive glasses which influences the cytotoxicity and anticancer activity have received attention in biomedical applications[27]. The efficient protein adsorption and drug delivery capability of bioactive glasses suggest that the size- and medium-dependent catalytic activity of lysozyme can be better utilized in many protein based applications and pharmaceutical industries.

In this paper, we report a systematic study on the size and surrounding dependent melting temperature, catalytic activity and glass transition temperature of a spherical virus using thermodynamical approaches. Furthermore, taking lysozyme as the protein coat in spherical virus is justified as it is a known powerful antibacterial protein widely distributed in various biological fluids and tissues including avian egg, plant, bacteria, tears, saliva, milk etc.

5.2 Methodology

To determine the size and temperature dependent thermodynamical parameters a unique approach based on the thermodynamics using size and shape terms is necessary. In this study, to model the size dependent thermodynamical properties such as melting temperature, catalytic activation energy and glass transition temperature, well-known Arrhenius equation is employed. The size and temperature dependent catalytic activation energy under the framework of Arrhenius equation can be expressed as[28];

$$K(D,T) = K_o(D)\exp\left(\frac{E_a(D)}{RT}\right) \quad (5.1)$$

where K_o is the pre-exponential factor. $E_a(D)$ expresses size dependent catalytic activation energy, R being the ideal gas constant and T is the temperature. Assuming the same average rate constant at the melting temperature for all viruses, we get the following expression to relate the catalytic activation energy and melting temperature[29].

$$\frac{T_m(D)}{T_m(\infty)} = \frac{E_a(D)}{E_a(\infty)} \tag{5.2}$$

where, $E_a(\infty)$is catalytic activation energy in bulk form, $T_m(D)$ is size dependent melting temperature and $T_m(\infty)$ is melting temperature of nanometric virus in bulk i.e. lysozyme protein crystal. The expression for the melting temperature of a nanoparticle (virus) embedded in a medium can be written as[30]

$$\frac{T_m}{T_{mb}} = \left[1 - \frac{3d\alpha}{2D}\left(1 - \frac{T_M}{T_{mb}}\right)\right] \tag{5.3}$$

Here, T_m is the melting temperature of virus nanoparticle with particular size (diameter), T_{mb} is the melting temperature of virus (lysozyme) in bulk, d is the actual diameter of virus and T_M is the melting temperature of the matrix (encircling medium). The α present in the above equation is shape factor and is considered equal to one for the spherical form.

The comparison of Equations 5.2 and 5.3 gives rise to the following expression,

$$T_m = T_m(D) \text{ and } T_{mb} = T_m(\infty) \tag{5.4}$$

Therefore, the catalytic activation energy using Equation 5.1 can be written as,

$$\frac{E_a(D)}{E_a(\infty)} = \left[1 - \frac{3d\alpha}{2D}\left(1 - \frac{T_M}{T_{mb}}\right)\right] \tag{5.5}$$

Equations 5.3 and 5.5, respectively will provide values of size dependent melting temperature T_m and catalytic activation energy E_a of an embedded spherical virus. These equations clearly reflect the effect of surrounding medium inclusion. Glycerol and water are the most common mediums in which viruses are present. In addition, the approach which will appear in what follows; the low-frequency studies on viruses have been performed with these surrounding mediums. It is clearly seen from above equations that the inclusion of surrounding mediums

modifies the expressions of these quantities, which can be attributed to the modification in cohesive energy of the free virus case.

According to Lindemann's criterion, a crystal melts when root mean square value of amplitude of thermal vibration (r) of atoms or molecules reaches a critical fraction of interatomic distances at particular temperature and expressed as[31];

$$\sigma^2(r,T) = F(r)\,T \tag{5.6}$$

In amorphous solids and glasses, calculations of the thermal conductivity at temperature above 50 K are well illustrated with a distinct model, due to Einstein, in which the harmonic motion of nearby atoms is uncorrelated. This model determines an elementary phenomenological depiction of the lattice vibrations in the frequency range of terahertz, and grants a quantifiable explanation of the heat transport. The heat capacity behavior of the glasses studied in the range 5–300 K is well described by the combination of Debye and Einstein heat capacity functions[32]. The Lindemann's model developed in 1910 for the study of melting transition is based on Einstein's explanation of the low temperature specific heat of crystals, $c_p(\infty)$ where the corresponding bulk characteristic Einstein temperature $\theta_e(\infty)$ is proportional to the Einstein frequency $\nu_E(\infty)$ as $\hbar\nu_E(\infty) = \theta_e(\infty)$. Here, $\hbar$ is the plank's constant. Lindemann's criteria has also been successfully applied to describe changes in the local dynamics of protein[33], atomic clusters[34] and polymer melts[35,36].

According to Shi's model for $T_m(r)$, the mean square displacement of a nanoparticle, $\sigma^2(r)$ can be presented as[37];

$$\frac{F(r)}{F(\infty)} = \frac{\{\sigma^2(r,T_m(r)/h^2)\}}{\{\sigma^2(\infty,T_m(\infty)/h^2)\}}\left[\frac{T_m(\infty)}{T_m(r)}\right] = \frac{T_m(\infty)}{T_m(r)} \tag{5.7}$$

Therefore, melting temperature, T_m can be written as;

$$\frac{T_m(r)}{T_m(\infty)} = \frac{\sigma^2(\infty)}{\sigma^2(r)} = exp\left\{\frac{-(\alpha-1)}{\left[\left(\frac{r}{r_o}\right)-1\right]}\right\} \tag{5.8}$$

where $\alpha = [2S_{vib}(\infty)/(3R)] + 1$

Since, glasses and crystals as solids have analogs structural characteristics of the short range order, they should possess the similar vibrational characteristics at their melting temperature. The glass transition temperature, T_g is deemed to be second order transition, therefore it can be acquired by substituting $C_{pg}(\infty)$ in place of S_{vib} in Equation (5.8), where $C_{pg}(\infty)$ is the heat capacity difference between the bulk glass and bulk liquid at $T_g(\infty)$. According to phenomenological observation, it is assumed that the $\sigma_g^2(\infty) \approx \sigma^2(\infty)$, where the subscript g denotes glass transition temperature, T_g. Replacing T_m (r), T_m (∞), $\sigma^2(r)$ and $\sigma^2(\infty)$ with T_g (r), T_g (∞), $\sigma_g^2(r)$ and $\sigma_g^2(\infty)$ in Equation (5.8), we obtain[29]

$$\frac{T_g(r)}{T_g(\infty)} = \frac{\sigma^2(\infty)}{\sigma^2(r)} = exp\left\{\frac{-(\alpha-1)}{\left[\left(\frac{r}{r_o}\right)-1\right]}\right\} \tag{5.9}$$

$r_o = c_1(3–d)h$, where d represents dimension; d=0 for nanosphere, d=1 for nanowires and d=2 for thin films. c_1 is the additional condition for different surface states which in case of nanocrystals is equal to unity.

As the virus is in the range of few nanometers like nanoparticles, the wavelength of low-frequency acoustic phonons is related to the atomic spacing, the virus nanoparticle can be treated as a uniform continuum sphere together with the isotropic medium[27]. The vibrational modes of a nanometric particle were first calculated by Lamb[38] by considering the acoustic vibrations of a particle as a whole from classical point of view and later by many others[9,39,40]. This requires sphere size, density and sound in corresponding bulk material as parameters to be used in calculation. The low-frequency vibrational modes are of two types: spheroidal and torsional modes. We have calculated the low-frequency vibration of spherical virus as this is analogous to semiconductor nanocrystals or quantum dots. The symmetry of the continuum model usually provides a series of good quantum numbers to identify the modes namely the spheroidal and torsional vibrational modes.

5.3 Size dependent melting temperature and catalytic activation energy of free and embedded virus

In this section we have compared our theoretical values using derived equations with the experimental values. Fig. 5.1 shows the size and matrix (water and glycerol) dependent melting temperature for spherical virus (lysozyme) which shows that the melting temperature rapidly decreases below 75-nm diameter similar to the other nanoparticles [41]. The T_m of virus without any medium is almost constant above 175nm and attains to the melting temperature of bulk lysozyme. We calculated melting temperature and presented in Table 5.1 together with the available experimental [42,43] and other theoretical data[36]. The obtained melting temperature of bulk lysozyme as 330 K is in good agreement with available experimental value obtained using differential scanning calorimetry (DSC) for chicken egg white lysozyme (CEWL) in the presence of perdeuterated matrices D_2O, glycerol and glucose [36]. While the experimental melting temperature for CEWL hydrated with 0.4 g water per gram of dry protein is 340 K, the same for CEWL embedded in 1:1 (gram protein per gram solvent) in glycerol and glucose is 370 K [36]. However in the same work from stability curves, they found melting temperature for two systems as $T_{m,sim}^{wat}$ = 444 K and $T_{m,sim}^{gly}$=524K[36]. This can be attributed to the convergence issues with atomistic force fields which generally overestimates the in silico melting temperature [44].

Fig. 5.1 also presents the size dependent melting temperature of spherical virus in two mediums water and glycerol, which shows a significant variation in the magnitude of melting temperatures as well as in the trend. Although there is an increase in melting temperature with size in the case of embedded virus, no rapid change is observed in melting temperature of embedded virus system. The melting temperature for both embedded systems at 200 K is about 25 K higher than the free virus, but the difference increases with lowering the temperature and is more than 100 K below 50 K. As far as two mediums glycerol and water are concerned the difference in melting temperature of virus is not very significant which can be seen from the inset of Fig.5.1. The melting temperature decrease of virus with size can be attributed to the increased surface-to-volume ratio of virus with its decreasing size[45] and

crystallinity of the structures[46]. However, when the virus is embedded in glycerol and water, the increase of melting temperature for a given size of virus can be attributed to the mismatch in the physical properties particularly the mechanical parameters and density of both virus particle and surrounding mediums[9]. However, in the case of virus embedded in glycerol and water, the lower value of T_m in the case of water embedded virus can be attributed to the formation of stronger hydrogen bonds[47] in polar water embedded viral protein and low cohesion energy due to less cohesion.

Table 5.1: Calculated values of melting temperature and glass transition temperature for free and embedded virus along with the other studies and experimental data.

	Melting temperature(T_m,K)			**Glass transition (T_g,K)**		
System	**Present**	**Exp**	**Other theories(MD)**	**Present**	**Exp**	**Other theories(MD)**
Lysozyme	330.1	340[42]	-	191.55, 289.59 [49]	130-240 [50], 280-313[51]	220[43], 215-245[53]
Lysozyme+ water	345.03	347.95 [48]	444[36]	286.4 [49]	150-170 [50]	-
Lysozyme+ glycerol	345.45	349.15[48], 370[36]	524[36]	281.3 [49]	175[52], 220[43]	-

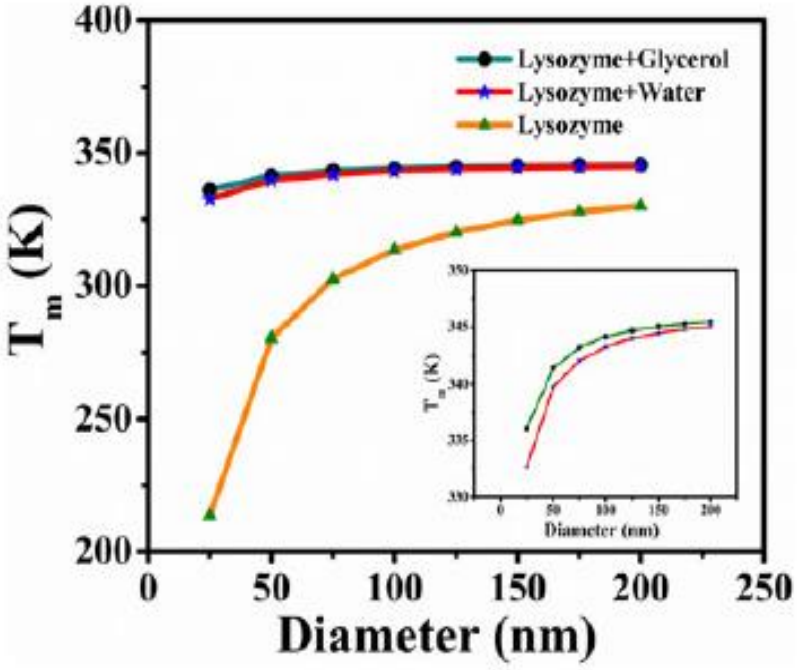

Figure 5.1: Size dependent melting temperature of free and embedded virus.

Table 5.2: Calculated values of catalytic activity for free and embedded virus along with the other studies.

	Catalytic activation energy (E_a,kj/mol)	
System	**Present**	**Others**
Lysozyme	88.53	-
Lysozyme+ water	92.52	75.3[50]
Lysozyme+ glycerol	92.63	-

Fig. 5.2 presents the size- and medium-dependent catalytic activation energy, E_a of considered spherical virus. The catalytic energy variation with size is similar to the melting temperature variation. All three curves representing three different cases show the decrease in E_a with decrease in size. The calculated catalytic activity energy for virus of about 200nm (bulk) in all cases presented in Table 5.2 clearly shows a good agreement with previous results [50]. In case of free virus the catalytic activation energy (E_a) is less than that of embedded virus. For water medium the catalytic activation energy is 89.2 kj/mol for 25nm virus which is higher than the same for 25nm free virus. This comparison shows that the virus embedded in water has less catalytic activation energy than that of glycerol medium and can be better in catalyzing any chemical reaction because less catalytic activation energy reveals to higher rate of chemical reaction. However, it is important to note that the free virus has lower catalytic activation energy. The catalytic activation energy value will be almost equal above 200nm size for both free and embedded cases.

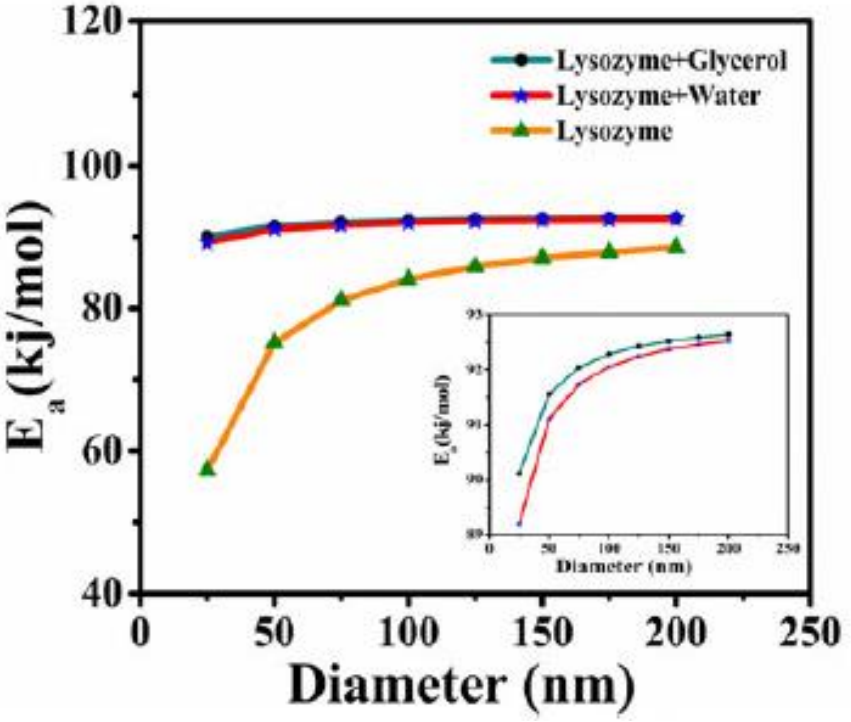

Figure 5.2: Size dependent catalytic activity of free and embedded virus.

5.4 Size dependent glass transition temperature of free and embedded virus

Fig. 5.3 shows the calculated results on the size dependent glass transition temperature T_g using the expression based on thermodynamics. Fig. 5.3 clearly depicts as size of virus increases there is a decrease in glass transition temperature T_g. It is interesting to note that the T_g/T_m ratio becomes more than one for the virus size of <50 nm in contrast to the usual trend in the polymer where it lies between 0.5 and 0.76 with a large majority of those with ratio 2:3[54]. This implies that the virus (material) behaves quite unsymmetrical for smaller size. However, for the size 150 nm the virus turns symmetrical as the T_g/T_m ratio is below 0.5[54]. This is in line of glass transition Lindemann criterion which shows $T_g \ll T_m$[55].

Table 5.1 clearly shows that the glass transition temperature for spherical virus composed of lysozyme protein is in good agreement with experimentally obtained values using DSC and dielectric measurements[43,50,51,52] and other theoretical calculations[43,53]. For the comparison we have also included data for myoglobin apart from the lysozyme which shows a good agreement between both.

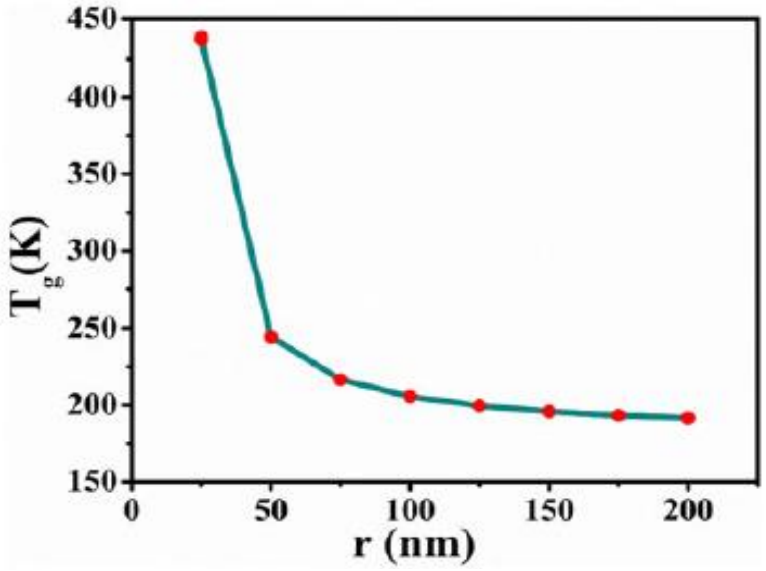

Figure 5.3: Size dependent glass transition temperature of free virus.

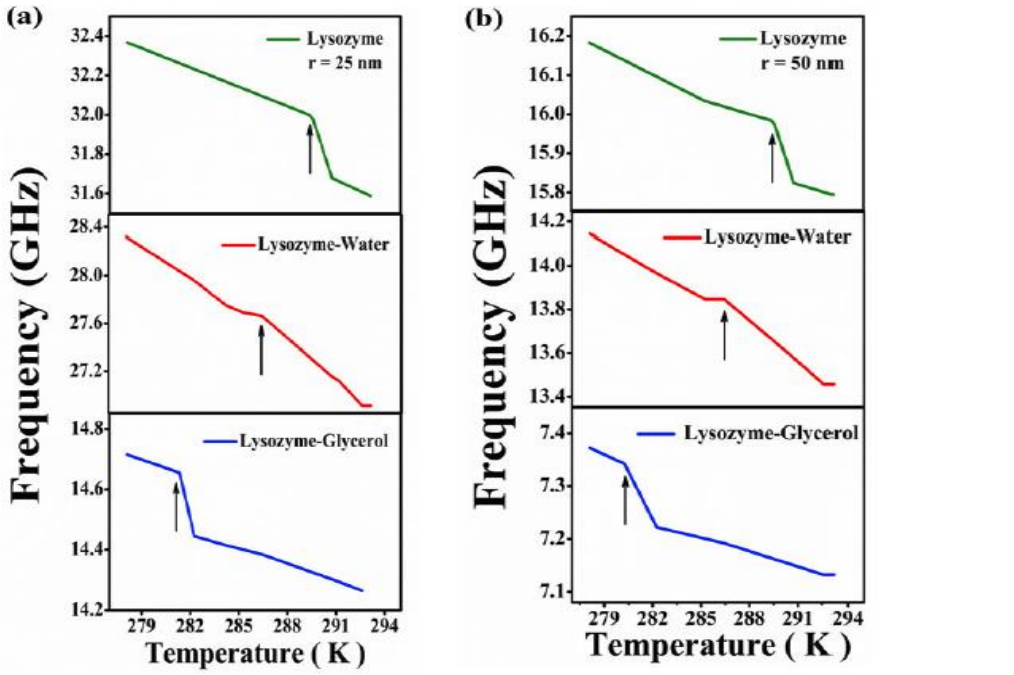

Figure 5.4: Temperature dependent low-frequency vibration curve for a free and embedded virus (a) for 25 nm and (b) 50 nm.

Fig. 5.4 presents the temperature versus frequency of Raman active low-frequency spheroidal phonon mode. The low-frequency Raman active mode is calculated using continuum approach. In addition, the structure of spherical viruses is quite suitable to be used as a material in continuum model. Viruses are composed of individual coat proteins bundled together to be approximately like a sphere. Each individual coat protein in the bundle comprises several amino acids. The calculation of properties using low-frequency mode based on elastic continuum model requires only two parameters, longitudinal and transverse sound velocities cl and ct; respectively of lysozyme as the measured speed of sound in different protein crystals is similar [9]. Furthermore, the approximation of treating virus as prefect spheres is not a drawback for the lowest lying acoustic phonon modes which are the only once that we calculate and use for the determination of properties particularly the glass transition temperature[56].

Furthermore, using the virus as homogeneous and isotropic object is justifiable as it has internal structure and without well-known anisotropicity. It is clearly seen from the Figure 5.4 that the nature changes sharply indicating a sharp glass transition. The sharp change in the temperature dependence of the frequency of the low-frequency mode have been used earlier to estimate T_g in some glass

formers[57,58]. However, the predicted value of T_g from temperature dependence of the low-frequency phonon mode is higher than the one obtained from thermodynamical calculation. This can be attributed to the fact that the low-frequency vibration is due to the whole vibration of the body. It is to be noted that the range of glass transition temperature which is obtained here is in good agreement with earlier measurements [59,50,60]. However, when virus of 50nm is embedded in medium such as water and glycerol, there is a decrease in T_g which may be attributed to the reduction in frequency due to damping of mode and radiating its vibrational energy to the water and glycerol.

5.5 Conclusions

This chapter presents the size dependent melting temperature, catalytic activation energy and glass transition temperature of the spherical virus by considering this as lysozyme protein crystal. All considered parameters show temperature dependency. Although the melting temperature and catalytic activation energy increases with decreasing size the glass transition temperature shows reverse behavior. In all cases the respective parameters attain the bulk value. The melting temperature is the required temperature which can be used to denaturate and kill the virus of a particular size. The calculated catalytic activation energy of spherical virus may have the implications in the field of catalyst. The calculated value of T_g for virus can be used to determine the elasticity or mechanical properties of the virus and hence mimicking the actual condition. This study also shows the effect of glycerol and water on these properties. The surrounding medium increases the melting temperature and catalytic activity energy but decreases the glass transition temperature. The glass transition temperature of virus has also been calculated using the temperature dependent low-frequency vibrational mode which shows a consistent result. This study also brings out the potential of this technique to be used as a complimentary technique for the determination of glass transition temperature of biological materials like virus and bacteria.

References

1. Q. A. Pankhurst, J. Connolly, S. K. Jones & J. Dobson, *Journal of Physics D: Applied Physics.* **36**, R167 (2003).

2. J. M. Alonso, M. L. Gorzny, A. M. Bittner, *Trends in Biotechnology*. **31**, 530 (2013)
3. C. E. Flynn, Lee, S. W. Peelle, B. R., & A. M. Belcher, *Acta Materialia*. **51**, 5867 (2003)
4. M. Gorzny, A. S. Walton, & S. D. Evans, *Advanced Functional Materials*. **20(8)**, 1295 (2010).
5. H. Park, N. Heldman, P. Rebentrost, L. Abbondanza, A. Iagatti, A. Alessi, A. M. Belcher, *Nature Materials*. **15(2)**, 211 (2016).
6. W. Shenton, T. Douglas, M. Young, G. Stubbs, S. Mann, *Advanced Materials*. **11(3)**, 253 (1999).
7. W.-J. Chung, J.-W. Oh, K. Kwak, B. Y. Lee, J. Meyer, E. Wang, A. Hexemer and S.-W. Lee, *Nature*. **478**, 364 (2011).
8. E. Ghavanloo & S. A. Fazelzadeh, *Mechanics of Advanced Materials and Structures*. **22(7)**, 597 (2015).
9. M. Talati, & P. K. Jha, *Physical Review E*. **73(1)**, 011901 (2006).
10. A. Aggarwal, E. R May, C. L. Brooks & W. S. Klug, *Physical Review E*. **93(1)**, 012417 (2016).
11. A. L. Bozic, A. Siber, *Biophysical Journal*. **115(5)**, 822 (2018).
12. C. Y. Zhang, N. H. Zhang, *Biophysical Journal*. **115(5)**, 763 (2018).
13. L. H. Ford, *Physical Review E*. **67**, 051924 (2003).
14. C. L. Jackson & G. B. McKenna, *Journal of Non-Crystalline Solids*. **131**, 221 (1991).
15. B. Jerome, *Journal of Physics: Condensed Matter*. **11(10A)**, A189 (1999).
16. Y. P. Koh, G. B. McKenna & S. L. Simon, *Journal of Polymer Science Part B: Polymer Physics*. **44(24)**, 3518 (2006).
17. Q. Jiang, H. X. Shi, J. C. Li, *Thin Solid Films*. **354(1–2)**, 283 (1999).
18. M. Siepi, J. Politi, P. Dardano , A. Amoresano, L. De Stefano, D. M. Monti, E. Notomista, *Nanotechnology*. **28(33)**, 335601 (2017).
19. J. G. Dash, *Reviews of Modern Physics*. **71(5)**, 1737 (1999).
20. S. K. Gupta, M. Talati, & P. K. Jha, *Materials Science Forum*. **570**, 132 (2008).
21. K. K. Nanda, *Pramana*. **72(4)**, 617 (2009).

22. T. Ku, P. Lu, C. Chan, T. Wang, S. Lai, P. Lyu, & N. Hsiao, *Computational Biology and Chemistry*. **33(6)**, 445 (2009).
23. C. Zhong, Y. Wang, G. Ma, R. Li, *Analytical Methods*. **8(18)**, 3809 (2016).
24. F. Mallamace, C. Corsaro, D. Mallamace, S. Vasi, C. Vasi, P. Baglioni, H. E. Stanley, *Proceedings of the National Academy of Sciences of the United States of America*. **113(12)**, 3159 (2016).
25. S. Chen, A. Kucernak, *The Journal of Physical Chemistry B*. **108(10)**, 3262 (2004).
26. L. Pauling, *Nature*. **161(4097)**, 707 (1948).
27. K. Zheng, M. Lu, Y. Liu, Q. Chen, N. Taccardi, N .Huser, A. R. Boccaccini, Biomedical *Materials*. **11(3)**, 035012 (2016).
28. S. Arrhenius, *Zeitschrift Fur Physikalische Chemie*. **4(1)**, 96 (1889).
29. H. M. Lu, & X. K. Meng, *The Journal of Physical Chemistry C*. **114(49)**, 21291 (2010).
30. W. H. Qi, & Wang, M. P. *Materials Letters*. **59(18)**, 2262 (2005).
31. Q. Jiang, & C. C. Yang, *Current Nanoscience*. **4(2)**, 179 (2008).
32. K. K. Mamedov, A. B. Abdullaev, B. Z. Shalumov, M. L. Mekhtiev, M. A. Alyanov, & D. O. Gumbatov, *Physica Status Solidi (A)*. **99(2)**, 413 (1987).
33. Y. Zhou, D. Vitkup, & M. Karplus, *Journal of Molecular Biology*. **285(4)**, 1371 (1999).
34. F. H. Stillinger & D. K. Stillinger, *Journal of Chemical Physics*. **93(8)**, 6013 (1990).
35. J. Dudowicz, K. F. Freed & J. F. Douglas, *The Journal of Physical Chemistry B*. **109(45)**, 21285 (2005).
36. M. Katava, G. Stirnemann, M. Zanatta, S. Capaccioli, M. Pachetti, K. L. Ngai, A. Paciaroni, *Proceedings of the National Academy of Sciences of the United States of America*. **114(35)**, 9361 (2017).
37. F. G. Shi, *Journal of Materials Research*. **9(5)**, 1307 (1994).
38. H. Lamb, *Proceedings of the London Mathematical Society*. **1**, 189 (1882).
39. E. Duval, *Physical Review B*. **46(9)**, 5795 (1992).

40. S. K. Gupta, S. Sahoo, P. K. Jha, A. K. Arora & Y. M. Azhniuk, *Journal of Applied Physics*. **106(2)**, 024307 (2009).
41. J. Sun & S. L. Simon, *Thermochimica Acta*. **463(1–2)**, 32 (2007).
42. E. Blanco, J. M. Ruso, J. Sabin, G. Prieto, F. Sarmiento, *Journal of Thermal Analysis and Calorimetry*. **87(1)**, 211 (2007).
43. P. J. Steinbach, B. R. Brooks, *Proceedings of the National Academy of Sciences of the United States of America*. **90(19)**, 9135 (1993).
44. L. L. Kresten, S. Piana, R. O. Dror, D. E. Shaw, *Science*. **334(6055)**, 517 (2011).
45. G. L. Allen, R. A. Bayles, W. W. Gile, W. A. Jesser, *Thin Solid Films*. **144(2)**, 297 (1986).
46. K. Koga, T. Ikeshoji, K. I. Sugawara, *Physical Review Letters*. **92(11)**, 115507 (2004).
47. S. B. Leslie, E. Israeli, B. Lighthart, J. H. Crowe, L. M. Crowe, *Applied and Environmental Microbiology*. **61(10)**, 3592 (1995).
48. T. Knubovets, J. J. Osterhout, P.J. Connolly and A.M. Klibanov, *National Acad. Sciences*. **96(4)**, 1262 (1999).
49. C.S. Tiwari, V. Sharma, P.K. Jha, A. Pratap, *Journal of Biomolecular Structure and Dynamics*. **38(8)**, 2207(2019)
50. V. N. Morozov, S. G. Gevorkian, *Biopolymers*. **24(9)**, 1785 (1985).
51. I. Teslyuk, Y. Vasylkiv, Y. Nastishin, R. Vlokh, *Ferroelectrics*. **346(1)**, 49 (2007).
52. H. Jansson, J. Swenson, *Biochimica et Biophysica Acta - Proteins and Proteomics*. **1804(1)**, 20 (2010).
53. K. Monkos, *International Journal of Biological Macromolecules*.**74**, 1 (2015).
54. W. A. Lee, G. J. Knight, *British Polymer Journal*. **2(1)**, 73 (1970).
55. J. C. Dyre, *Reviews of Modern Physics*. **78(3)**, 953 (2006).
56. D. B. Murray & L. Saviot, *Journal of Physics: Conference Series*. **92(1)**, 012036(2007)
57. J. A. Forrest, K. Dalnoki-Veress & J. R. Dutcher, *Physical Review E*. **56(5)**, 5705(1997).

58. F. Terki, C. Levelut, J. L. Prat, M. Boissier & J. Pelous, *Journal of Physics: Condensed Matter*. 9(19), 3955 (1997).

59. J. L. Green, J. Fan & C. A. Angell, *The Journal of Physical Chemistry*. **98(51)**, 13780(1994).

60. G. Sartor, E. Mayer & G. P. Johari, *Biophysical Journal*, **66(1),** 249(1994).